Journal of Visualization, Vol. 9, No. 2 (2006)199-208

Direct Measurement of Fluid Velocity Gradients at a Wall by PIV Image Processing with Stereo Reconstruction

Nguyen, C. V.*[1] and Wells, J. C.*[2]

*1 Department of Civil & Environmental Engineering, Ritsumeikan University, Kusatsu, Shiga 525-8577, Japan. E-mail: jwells@se.ritsumei.ac.jp
*2 Currently Department of Mechanical Engineering, Monash University, Clayton, Victoria 3800, Australia.

Received 17 June 2005
Received 21 October 2005

Abstract : Velocity gradient is typically estimated in Particle Image Velocimetry (PIV) by differentiating a measured velocity field, which amplifies noise in the measured velocities. If gradients near a boundary are sought, such noise is usually greater than in bulk fluid, because of small tracer displacement, uncertainty in the effective positions of velocity vectors, intense deformation of tracer patterns, and laser reflection. We consider here a modified form of the Particle Image Distortion (PID) method to *directly* calculate velocity gradients at a fixed wall, and refer it as "PIV/IG" ("Interface Gradiometry"). Results from synthetic 2D PIV images suggest our method achieves higher SNR and accuracy than velocity differentiation. Also, we have developed a procedure to reconstruct three-dimensional velocity gradient at a fixed wall the two non-zero components from PIV/IG data obtained in stereo views; these equations simplify considerably thanks to the no-slip condition. Experimental data from the bottom wall of turbulent open channel flow appear to suffer from a form of pixel locking. As with standard PIV, this underlines the importance of adequate tracer diameter in the images, sufficient seeding density, and of dynamic range of the camera sensor.

Keywords : PIV, PID, Stereo reconstruction of velocity gradient, Wall velocity gradient, Synthetic image.

1. Measuring Interfacial Gradients

Velocity gradients at a phase boundary determine the viscous boundary stress, and correlate strongly with heat and chemical fluxes, so it is important to measure them accurately in turbulent flow. To validate models for wall-stress and mass transfer in Large Eddy Simulation, our group will apply PIV to measure statistics of wall shear stress, and surface divergence at a free surface, in turbulent channel flow. We further aim to relate boundary gradients to nearby vortical structure. This contribution describes a technique developed for that purpose.

Particle Image Velocimetry (PIV) yields velocities throughout a light sheet. In principle, these velocities might be differentiated to yield the field of velocity gradients, including values at a wall or other interface. There are however numerous difficulties in applying standard PIV near a wall or fluid phase boundary (not to mention taking differences of such a signal!). First, the signal level is low; near a fixed wall, both components approach zero. Second, especially at the wall, one must resolve high gradients in thin layers. Where most sensors would yield a deterministically smoothed value of the measurand in the sensing region, Pattern Matching PIV produces a raw signal, the correlation map, which is a *union* of particle matches and mismatches at random locations through

the sensing volume. Thus, the effective position of measured PIV velocity vectors, typically dominated by the positions of the brightest tracer particles, is unknown; this is especially unwelcome in a thin shear layer such as found at a wall, when one wants to determine velocity gradients. This communication suggests how to surmount these difficulties with a modified version of Pattern Image Distortion (PID) technique (Huang et al., 1993), in this case by shearing PIV image templates parallel to a no-slip wall. We refer to this enhancement to PIV as "Interface Gradiometry", abbreviated PIV/IG. We have also been developing this technique for flow at free surface, as reported separately in Phan et al. (2005).

The PID method was first proposed by Huang et al. (1993) to improve the accuracy of standard PIV interrogation for high velocity gradient regions. At first, standard cross-correlation is done to estimate velocity gradients, then images are distorted so as to compensate the estimated deformation. The process is iterated until convergence is achieved. The PID concept has subsequently been refined by many authors and is now exploited in commercial PIV software; please refer to Scarano (2002) for a detailed review.

While the principal purpose of the above-mentioned works was to increase S.N.R. of *velocity* measurements, some authors have aimed at direct measurement of velocity *gradient.* Ruan et al. (2001) performed cross correlation of the polar coordinate transformation of particle image patterns thus achieving fast and accurate measurement of vorticity, together with velocity components. Hart (2002) proposed to generate a four-dimensional correlation table, whose parameters were the two shear components of velocity gradient in addition to the usual two velocity components. Hart's emphasis on *directly* determining velocity gradients inspired the work reported herein. Although measurement of shear at a fixed wall would appear to be an obviously beneficial application of PID as adapted for direct measurement of gradients, we find no such report in the literature aside from our preliminary communication (Nguyen and Wells, 2003(a)).

The present paper describes results of validation tests for PIV/IG, using synthetic PIV images near a fixed wall. Image templates are anchored at the wall and sheared by varying degrees, and the problem for a single camera is then a *one-dimensional* pattern-matching problem whose only parameter is the projection of wall shear in the viewing direction. We then describe stereo reconstruction of such projected wall gradients, and investigate the accuracy of reconstructed gradients by synthetic images. Finally we present experimental data from Stereo PIV/IG in a turbulent open channel flow. By simultaneously applying PIV, possibly enhanced by PID, to measure velocity throughout a light sheet and PIV/IG to record instantaneous profiles of velocity gradient along a solid boundary, we hope to extend considerably the capability to visualize interfacial dynamics.

2. Near-Wall Image Gradiometry

This section describes how to measure the velocity gradient seen at a fixed wall by a single camera viewing parallel to the wall and perpendicular to the light sheet. We assume sufficient resolution that the instantaneous velocity profiles near the wall are approximately linear over the height of a template, which we find requires about 3 or more pixels per wall unit, and template heights less than about 4 wall units.

Physical coordinates and velocity will be denoted by (x: streamwise, y: vertical, z: spanwise) and (u, v, w) respectively. We assume no slip at the wall,

$$u = v = w = 0 \tag{1}$$

so tangential velocity derivatives vanish. In particular, $\partial u/\partial x = \partial w/\partial z = 0$, and if the flow is incompressible then $\partial v/\partial y = 0$. The only non-zero velocity gradients to be determined are then $\partial u/\partial y$ and $\partial w/\partial y$.

$$\frac{\partial u}{\partial x} = \frac{\partial u}{\partial z} = \frac{\partial v}{\partial x} = \frac{\partial v}{\partial y} = \frac{\partial v}{\partial z} = \frac{\partial w}{\partial x} = \frac{\partial w}{\partial z} = 0 \tag{2}$$

Pixel coordinates are denoted by *(X, Y)*, and projected components of interimage displacement by *(U, V)*. Assume that the wall appears horizontal on the image, and that magnification m is constant: $(X, Y, U, V) = m\,(x, y, u\Delta t, v\Delta t)$. The rate of shear $\partial u/\partial y$ is measured through its imaged projection $\partial U/\partial Y$, which is estimated by searching for the maximum of the cross- correlation coefficient:

$$C_{\frac{\partial U}{\partial Y}} = \frac{\sum_{m=1}^{M}\sum_{n=1}^{N}\left[\left(I_{m+n\frac{\partial U}{\partial Y},n} - \bar{I}_{\frac{\partial U}{\partial Y}}\right)\left(I'_{m,n} - \bar{I}'\right)\right]}{\sqrt{\sum_{m=1}^{M}\sum_{n=1}^{N}\left(I_{m+n\frac{\partial U}{\partial Y},n} - \bar{I}\right)^2}\sqrt{\sum_{m=1}^{M}\sum_{n=1}^{N}\left(I'_{m,n} - \bar{I}'\right)^2}} \tag{3}$$

$$\bar{I}_{\frac{\partial U}{\partial Y}} = \frac{1}{MN}\sum_{m=1}^{M}\sum_{n=1}^{N} I_{m+n\frac{\partial U}{\partial Y},n} \qquad \bar{I}' = \frac{1}{MN}\sum_{m=1}^{M}\sum_{n=1}^{N} I'_{m,n}$$

Instead of *translating* templates from the first image before correlating with the second, as in PIV, they are *sheared* parallel to the wall by a range of trial values. Bi-cubic interpolation of pixel intensity is used in resampling the sheared templates, which are then cross-correlated with the second image as in Eq. (3). The measured $\partial U/\partial Y$ corresponds to the peak of the correlation curve (*cf.* Fig. 1), as determined by a 3-point Gaussian fit. In practice, digital masking (Gui et al., 2003) is applied to cut out boundary reflections, but this refinement is not included in Eq. (3).

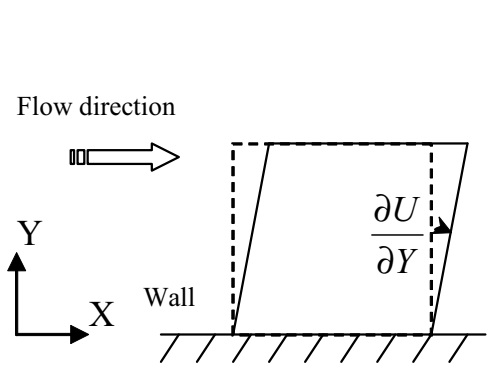

Fig. 1. Linear shear deformation adjacent to a fixed wall, as projected onto image sensor.

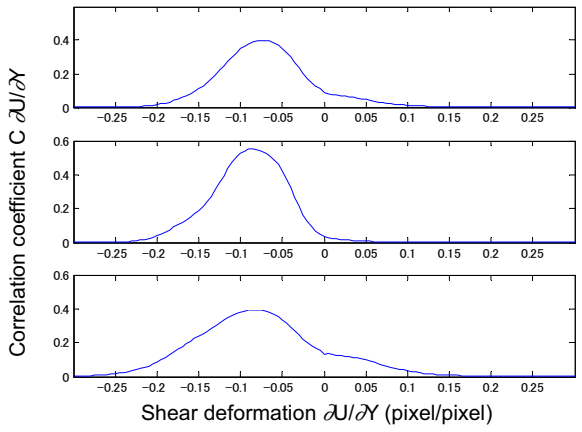

Fig. 2. PID correlation curves (Eq. (3)) at 3 neighboring boundary points, from an image pair in the stereo PIV experiment presented in Figs. 8-10. Template size is 80 × 20 pixels (14.5 × 3.6 wall units^2), delay between exposures is 5 ms.

By comparison, PID (Huang et al, 1993) deforms templates according to differentiation of a velocity field initially measured by standard PIV.

The wall will never be perfectly horizontal or vertical in real images. Local axes $(\tilde{X}, \tilde{Y})$ aligned with the wall can be used to calculate the normal gradient $\frac{\partial \tilde{U}}{\partial \tilde{Y}}$. In practice, pixel coordinates can be used directly, and considerable programming can be avoided, by aligning pixel lines closely with a wall. For example if the alignment is to within 1 degree, $\frac{\partial \tilde{U}}{\partial \tilde{Y}} \cong \frac{\partial U}{\partial Y}$ to an accuracy of 0.03 %.

3. Validation by 2D Synthetic Images

Synthetic PIV images were produced based on a single known velocity field from a Navier-Stokes simulation of turbulent open-channel flow ($Re_\tau = 300$), using a 64^3 grid on a domain with a height:

width : length ratio of 1 : 1.92 : 3.84. Although this grid does not qualify the simulation as fully resolved, it suffices for the purpose of PIV/IG validation; we refer this velocity field as "DNS data". Fig. 3(a)-(b) show velocity gradient profiles from DNS which varies widely in both the streamwise and wall-normal directions. A set of 20 synthesized image pairs was generated from the same DNS velocity field in a streamwise-vertical plane. Tracer images are taken to have a Gaussian profile with diameters from 3 to 6 pixels, and peak intensities from 100 to 200. Seeding density is 0.064 tracer/pixel^2, about the same as the normal tracer density used for PIV-STD Project's images (Okamoto et al., 2000). Particle displacements are about 10 pixels far from the wall, and about 2 pixels at $y^+ = 5$. Streamwise profiles of wall gradient in each image pair were calculated directly by PIV/IG.

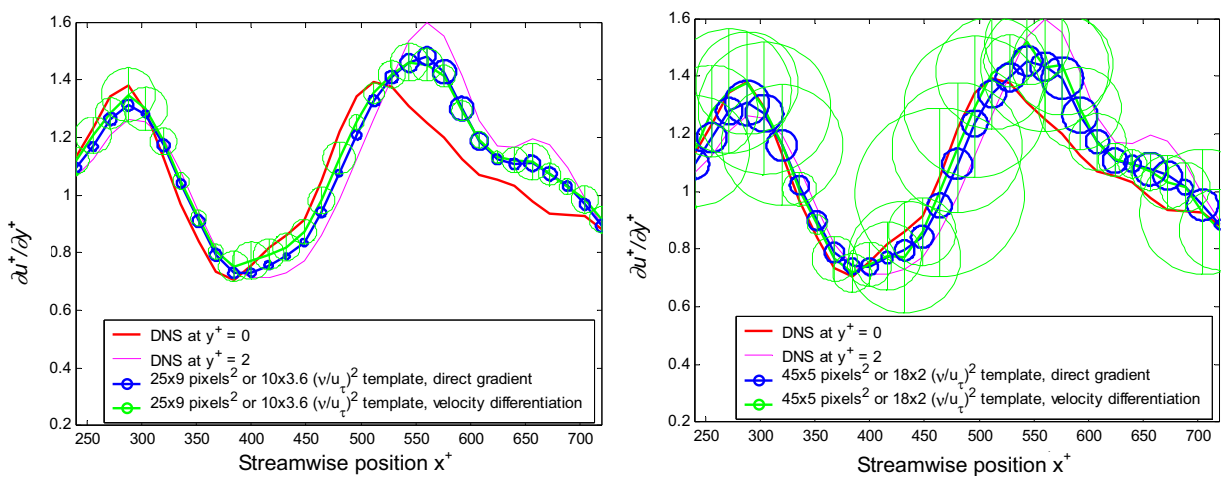

(a) Template size of 25 × 9 pixels (10 × 3.6 wall units^2)

(b) Template size of 45 × 5 pixels (18 × 2.0 wall units^2)

Fig. 3. Instantaneous streamwise profiles of wall gradient $\partial u^+/\partial y^+$ component from DNS, with PIV/IG, and differentiation of PIV/PID velocities obtained from synthetic images from DNS velocity field. Average tracer count in a template is 14.2.

For comparison, we also calculated wall velocity gradient corresponding to velocity obtained from PIV/PID with the same image templates used for PIV/IG. This implementation of PIV/PID is a 2D cross-correlation: image templates are distorted over a range of shear (instead of a single value estimated from velocity field calculated without distortion), and shifted along the wall. When the distortion compensates gradient, the correlation table is maximal. Velocity is obtained by a Gaussian fit. When differentiating velocity, the distance was taken from the template center to the wall. The same trial values of shear deformation were applied in PIV/IG and PIV/PID.

For each method, the measurements vary from one synthetic image pair to another. The radii of circles in the figures represent the r.m.s. fluctuation, and the continuous lines the local sample means of the 20 measurements at each location. Figure 3(a) shows a near-optimal selection of template size, 10 wall units wide × 3.6 wall units high, yielding 14.2 tracers per template on average. In Fig. 3(b), template height is reduced, with template width increased to keep the same area and number of tracers. This makes the mean profiles of both methods approach the DNS profile for $y^+ = 0$, but it increases the r.m.s. fluctuation of the measurements. Conversely, increasing template height may reduce the r.m.s. fluctuation but, when increased above 4 wall units, the profiles of sample means differ considerably from the DNS gradients at $y^+ = 0$. In both figures, PIV/IG is more accurate than the velocity differentiation method.

4. Stereo Reconstruction of Gradients

Figure 7 is a schematic top view of the two-camera Stereo PIV setup in our laboratory (Wells et al., 2003) which employs two Scheimpflug cameras in Willert's (1997) front-and-rear configuration. Each camera provides 2 components of velocity. At a given position in the light sheet, the two cameras

provide 4 measured velocity components, which thus overdetermine the velocity vector of 3 physical components (*cf.* Eq. (7) below). This problem is solved by a least-squares method. As we will now show, a nearly identical procedure can be followed to reconstruct wall velocity *gradients*.

First, write the mapping function between physical space *(x, y, z)* and image space *(X, Y)* as:

$$\begin{aligned} X &= X(x, y, z) \\ Y &= Y(x, y, z) \end{aligned} \tag{4}$$

For our apparatus, we have found that a linear "generalized pinhole" camera model is suitable (Wells et al., 2003).

During a time interval Δt, a tracer with displacement $(\Delta x, \Delta y, \Delta z)$ is projected onto the camera sensor with displacement $(\Delta X, \Delta Y)$ according to the formula:

$$\begin{aligned} \Delta X &= \frac{\partial X}{\partial x}\Delta x + \frac{\partial X}{\partial y}\Delta y + \frac{\partial X}{\partial z}\Delta z \\ \Delta Y &= \frac{\partial Y}{\partial x}\Delta x + \frac{\partial Y}{\partial y}\Delta y + \frac{\partial Y}{\partial z}\Delta z \end{aligned} \tag{5}$$

Dividing the equation by Δt yields:

$$\begin{aligned} U &= \frac{\partial X}{\partial x}u + \frac{\partial X}{\partial y}v + \frac{\partial X}{\partial z}w \\ V &= \frac{\partial Y}{\partial x}u + \frac{\partial Y}{\partial y}v + \frac{\partial Y}{\partial z}w \end{aligned} \tag{6}$$

where U and V are apparent velocity in image space (i.e., pixel/sec) while u, v and w are velocity components in physical space. Denoting each of the 2 stereo cameras by superscripts (I) and (II), the velocity reconstruction equation is:

$$\begin{bmatrix} U^{(I)} \\ V^{(I)} \\ U^{(II)} \\ V^{(II)} \end{bmatrix} = \begin{bmatrix} \frac{\partial X^{(I)}}{\partial x} & \frac{\partial X^{(I)}}{\partial y} & \frac{\partial X^{(I)}}{\partial z} \\ \frac{\partial Y^{(I)}}{\partial x} & \frac{\partial Y^{(I)}}{\partial y} & \frac{\partial Y^{(I)}}{\partial z} \\ \frac{\partial X^{(II)}}{\partial x} & \frac{\partial X^{(II)}}{\partial y} & \frac{\partial X^{(II)}}{\partial z} \\ \frac{\partial Y^{(II)}}{\partial x} & \frac{\partial Y^{(II)}}{\partial y} & \frac{\partial Y^{(II)}}{\partial z} \end{bmatrix} \begin{bmatrix} u \\ v \\ w \end{bmatrix} \tag{7}$$

where we abbreviate in matrix notation as $[U] = [M][u]$. Generalization to three or more cameras is obvious. Differentiation of (7) gives:

$$\frac{\partial [U]}{\partial x_i} = \frac{\partial [M]}{\partial x_i}[u] + [M]\frac{\partial [u]}{\partial x_i} \tag{8}$$

Again taking the wall to lie in the *(x, z)* plane, and invoking the non-slip boundary condition for velocity and the resulting conditions (2) for velocity gradients, this equation simplifies to

$\frac{\partial [U]}{\partial y} = [M]\frac{\partial [u]}{\partial y}$, or:

$$\begin{bmatrix} \frac{\partial U}{\partial y}^{(I)} \\ \frac{\partial V}{\partial y}^{(I)} \\ \frac{\partial U}{\partial y}^{(II)} \\ \frac{\partial V}{\partial y}^{(II)} \end{bmatrix} = \begin{bmatrix} \frac{\partial X}{\partial x}^{(I)} & \frac{\partial X}{\partial y}^{(I)} & \frac{\partial X}{\partial z}^{(I)} \\ \frac{\partial Y}{\partial x}^{(I)} & \frac{\partial Y}{\partial y}^{(I)} & \frac{\partial Y}{\partial z}^{(I)} \\ \frac{\partial X}{\partial x}^{(II)} & \frac{\partial X}{\partial y}^{(II)} & \frac{\partial X}{\partial z}^{(II)} \\ \frac{\partial Y}{\partial x}^{(II)} & \frac{\partial Y}{\partial y}^{(II)} & \frac{\partial Y}{\partial z}^{(II)} \end{bmatrix} \begin{bmatrix} \frac{\partial u}{\partial y} \\ \frac{\partial v}{\partial y} \\ \frac{\partial w}{\partial y} \end{bmatrix} \tag{9}$$

This has exactly the same form as the original reconstruction Eq. (7) for velocity, and may be solved by least squares analogously for the unknown $\partial[u]/\partial y$. For this purpose, the left side of Eq. (9) is expanded in terms of measured quantities as follows:

$$\begin{aligned} \frac{\partial U}{\partial y} &= \frac{\partial U}{\partial X}\frac{\partial X}{\partial y} + \frac{\partial U}{\partial Y}\frac{\partial Y}{\partial y} \\ \frac{\partial V}{\partial y} &= \frac{\partial V}{\partial X}\frac{\partial X}{\partial y} + \frac{\partial V}{\partial Y}\frac{\partial Y}{\partial y} \end{aligned} \tag{10}$$

For each camera, the gradients with respect to camera pixel coordinates, $\frac{\partial U}{\partial X}, \frac{\partial U}{\partial Y}, \frac{\partial V}{\partial X}$ and $\frac{\partial V}{\partial Y}$, can be obtained geometrically from the gradient of tangential velocity in the local wall normal direction, $\frac{\partial \tilde{U}}{\partial \tilde{Y}}$. Equation (10) yields $\frac{\partial U}{\partial y}$ and $\frac{\partial V}{\partial y}$, which are then plugged into Eq. (9).

5. Validation by Stereo Synthetic Images

We have developed a program that simulates the Stereo PIV system shown in Fig. 7, (Wells et al., 2003) discussed in the next section. Lens aberration and other environmental effects are neglected in the simulation program. DNS velocity data is interpolated from a 64^3 grid to randomly positioned tracers as in the 2D validations.

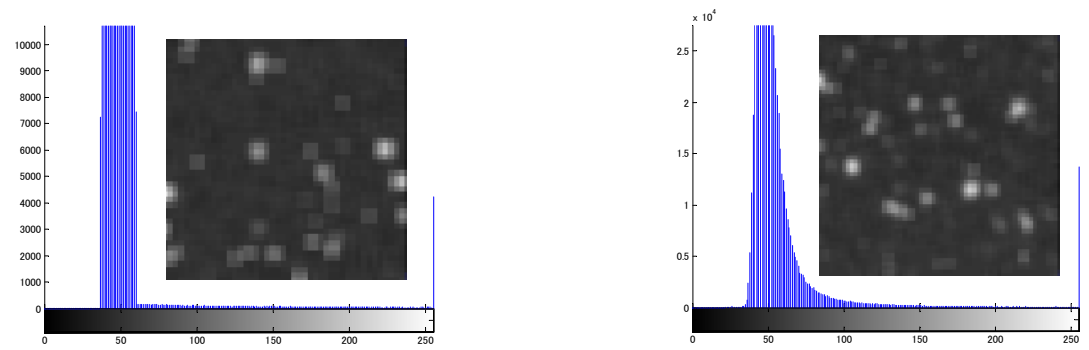

(a) Synthetic-image intensity histogram (b) Experimental-image intensity histogram

Fig. 4. Comparison of intensity histogram between synthetic image and experimental images (The size of the 2 image samples is 60 x 60 pixels).

As before, 20 images pairs are generated from the same DNS velocity data for each camera. Re_τ is 150 at a flow depth of 30 mm. The cross-stream laser sheet is 2 mm thick, and the average particle displacement perpendicular to the laser sheet is about 0.5 mm, so roughly 75 % of particles

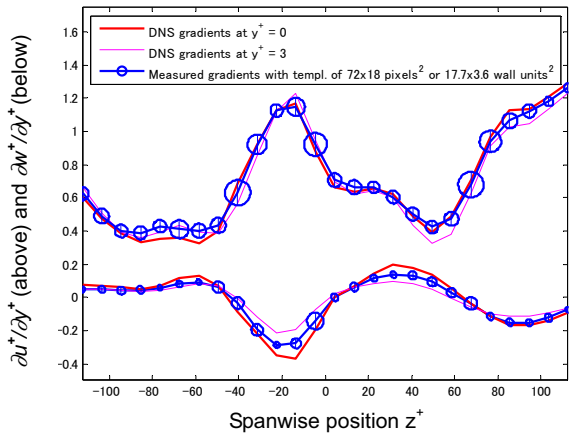

Fig. 5. Instantaneous streamwise profiles of wall gradient $\partial u^+/\partial y^+$ and $\partial w^+/\partial y^+$ components from synthetic stereo image pairs with PIV/IG using a template size of 72 × 18 pixels, or 17.7 × 3.6 wall units^2. The radii of circles in the figures represent the RMS deviation, and the continuous lines the local sample means of the 20 measurements at each location as compared with exact ("DNS") values.

are common to an image pair. However, close to the wall, the percentage of common tracer particles can be as high as 90 % or more due to low velocity. Simulated Scheimpflug cameras with a resolution of 1400 × 250 pixels look from the 2 sides of the laser sheet at 30 degrees from the normal direction and see a region of about 60 × 10 mm^2. The cameras are positioned so that the bed of the channel appears precisely horizontal in the camera images. Particles are generated randomly in a volume containing the laser sheet, and are projected onto each camera's sensor to obtain image coordinates. The projection matrix includes the apparent axial compression (Nguyen and Wells, 2003a) resulting from the change in refractive index at the surfaces of viewing prisms. Laser sheet intensity is assumed to have a Gaussian profile from 250 to 800 in grey scale so most tracers are saturated, as in experimental images. (In practice Nd-YAG laser sheets are often very non-Gaussian due to hot and cold spots in the beam). Tracer size is from 1 to 3 pixels in diameter. Tracer density is about 0.011 tracer/pixel, the same as for the experimental images analyzed in section 6. Pixel images of particles are generated with a random background noise. This background noise and tracer image saturation makes the synthetic images look similar to that of experimental images (*cf.* Fig. 4) (although the intensity histograms appear somewhat different, these synthetic images are more realistic than any we could find in current literature).

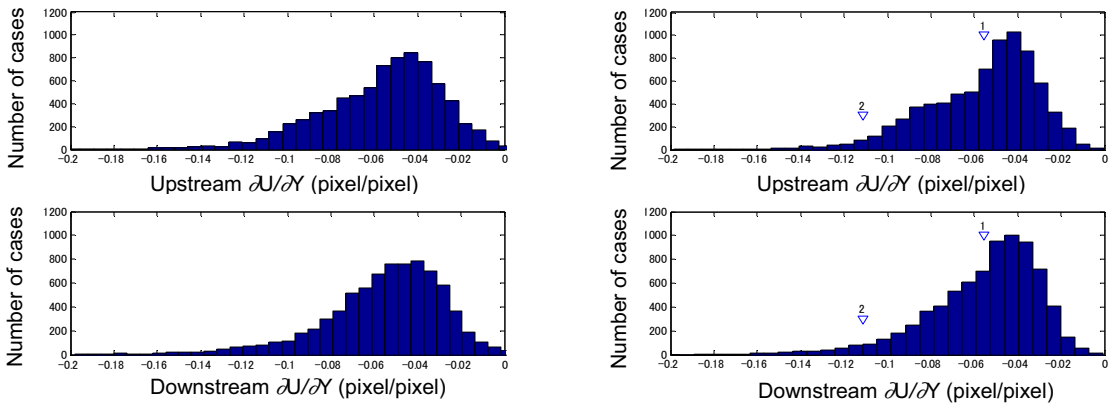

(a) DNS image gradients

(b) Simulated image gradients using template of 72 × 18 pixels (17.7 × 3.6 wall units^2)

Fig. 6. Histograms of image gradient directly from projection of DNS data, and calculated from synthetic images. The triangles denote the gradient caused by a pixel displacement of 1 and 2 pixels at the top edge of template. Seeding density is 0.011 tracers/pixels.

Velocity gradients are calculated from the image pairs of each camera using a template size of 72 × 18 pixels, about 17.7 × 3.6 (wall units)², and are reconstructed as described above to produce 2 components of wall velocity gradient. Figure 5 shows instantaneous profiles of reconstructed velocity gradient. We can see both horizontal and vertical smoothing effects. From the low-pass filter effect in the horizontal, when the DNS gradient goes to maximum, it is higher than the measured gradient. The opposite is also true when DNS gradient goes to minimum. As a result of the vertical averaging effect, the measured gradients tend to lie between gradients at $y^+ = 0$ and $y^+ = 3$.

Figure 6 shows the histograms of 300 projected velocity gradients for the two cameras. These will be compared with corresponding experimental histograms in the next section.

6. Stereo PIV/IG Experiments

Stereo PIV experiments have been performed in a 0.5 m wide × 8 m long water channel as shown in Fig. 7. In the runs presented here, flow depth was 60 mm, water temperature was 11 °C and discharge was 3.324 liters/s. The laser illuminates a cross-stream sheet about 1.7-2 mm thick. Two 1K² Kodak ES 1.0 cameras view horizontally, at about 30° from the upstream and downstream directions, through prisms on the channel wall. Frame rate is 30 Hz, and frame straddling with a 5.0 ms delay yields velocity fields at 15 Hz. A glass bottom wall greatly reduces laser reflection, and any remaining reflection line is eliminated by masking (Gui et al, 2003). The Reynolds shear stress profile was extrapolated to obtain a friction velocity of 0.765 cm/s, yielding $Re_\tau = 358$. A displacement within the light sheet of 1 mm, or 6 wall units, roughly corresponds to 22 pixels horizontally and 27 pixels vertically in the images.

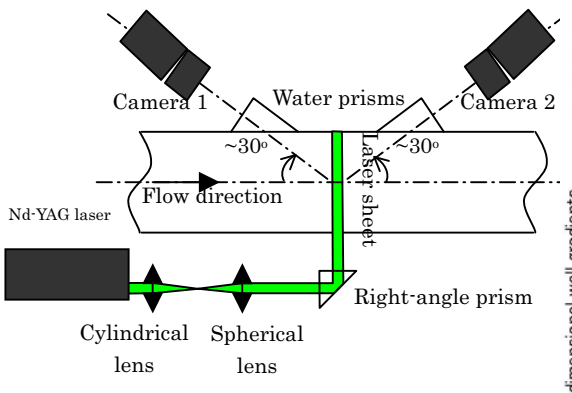

Fig. 7. Schematic view of Stereo PIV system (Wells et al., 2003).

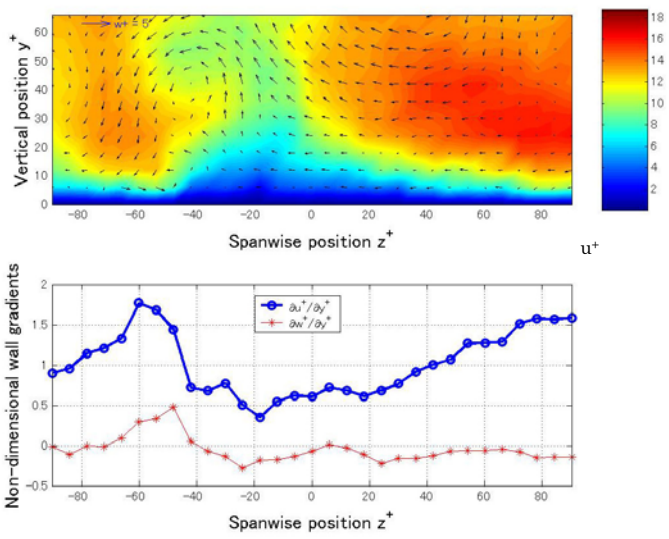

Fig. 8. Instantaneous 3-C velocity field and streamwise and spanwise gradient profiles from experiment. The background color represents streamwise velocity component u^+.

Wall velocity gradient was calculated by PIV/IG using 68 × 17 pixels templates, equivalent to 18.5 × 3.8 (wall units)². The tracer density is 0.011 tracers/pixel. Instantaneous profiles of the reconstructed wall velocity gradients, with the corresponding 3-C velocity field calculated using 33 × 33 pixels templates are shown in Fig. 8.

Based on a sample of 1400 image pairs saved at 1 Hz, Fig. 9 shows histograms of the apparent rate of shear seen by the two cameras. The range of the graph coincides with that of PIV/IG interrogation, with steps of 0.005 pixel/pixel. The graphs show a very clear peak in the bin just to the right of -0.05, and other clear biases towards values near -0.1, -0.15, -0.2. This effect strongly suggests some type of pixel locking, which in standard PIV is the bias toward integer values of tracer displacement that occurs when tracer images have an intensity distribution less than about two pixels wide. We argue that this occurs in PIV/IG when tracer density is low and tracer size is small

(1-2 pixels), as follows. First, consider the correlation peak in the extreme case in which only one tracer particle lies somewhere in the template. Shearing the template shifts the tracer's intensity profile in proportion to its height, and correspondingly the width of the 1D correlation curve (*cf.* Fig. 2), will be inversely proportional to the tracer's height. Thus, tracer particles near the top of the template, because of their narrower correlation peaks, will dominate the measurement of shear rate. Accordingly, we hypothesize that the biases in the histogram are toward pixel values of displacement for tracer particles near the top edge of the template. In Fig. 9, the triangles indicate rates of shear giving displacements of 1, 2, 3, and 4 pixels in the top row of the template, and these do indeed lie near the "biased bulges" in the histograms. Although we would expect, from the above discussion, for such bulges to lie to the left of the triangles, rather than slightly rightward as observed, the overall correspondence leaves little room for doubting our hypothesis. Comparing histograms in Fig. 6 (a)-(b), we can see similar "biased bulges" exist in the "measurements" from synthetic images. We believe such bias is caused by saturated small tracers and low tracer density. In experiment the bias is more severe possibly because about 1/4-1/3 of the template area is randomly cut off due to reflection masking.

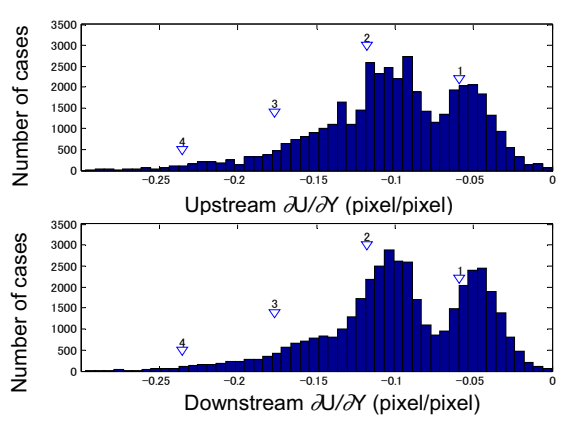

Fig. 9. Histograms of wall velocity gradient in experimental images of upstream and downstream cameras.

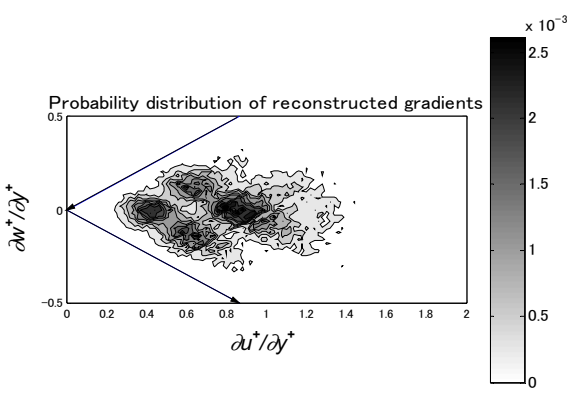

Fig. 10. 2D histogram of wall-velocity gradient; arrows show viewing directions of the down- and upstream cameras.

Figure 10 shows the two-dimensional histogram of the rate of bed shear. The biases observed in the 1D histograms yield streaks along the viewing directions of the two cameras, and such bias clearly limits the value of this experimental frequency distribution. In view of this bias, our eyeballed error estimates for the low-order moments of the distribution in Fig. 10 are 4 % for the mean, 10 % for the r.m.s. fluctuation of $\partial u/\partial y$, and 15 % for the r.m.s. fluctuation of $\partial w/\partial y$.

7. Conclusion

The "PIV/IG" technique proposed here is an extension to PIV for direct measurement of shear rate at a fixed wall. It has been validated by synthetic PIV images in a standard 2-component PIV configuration. The results suggest that this technique is superior to differentiation of conventional PIV data for measuring velocity gradients at an interface. Like standard PIV, the accuracy and resolution depend on the choice of template size, particularly its height. In general, as height gets smaller, the velocity gradient approaches the exact value at the interface if there are sufficient tracer images in each template. However, excessively small template height yields larger random error, and bias due to low tracer displacement.

Preliminary data from stereo PIV/IG at the bottom wall of open-channel flow show that pixel locking remains as much an issue as with standard PIV. In future work, we hope to improve our experimental technique so as to mitigate the effects of pixel locking.

Acknowledgements

The research reported herein was partially supported by a Grant-in Aid for Scientific Research of the MEXT Ministry of Japan, and by the Environmental Flows Research Group at Ritsumeikan University. Thanks go to Mr. T.X. Dinh, in the CFD Laboratory of Ritsumeikan University for advice on DNS of turbulent channel flow.

References

Fincham, A. and Delerce, G., Advanced optimization of correlation imaging Velocimetry algorithms, Exp. Fluids 29 (2000), 13-22.

Gui, L., Wereley S. T. and Kim H. Y., Advances and applications of the digital mask technique in particle image velocimetry experiments, Meas. Sci. Technol., 14 (2003), 1820-1828.

Hart, D., PIV processing using multidimensional correlation, 10th International Symposium on Flow Visualization (Kyoto, Japan), (2002).

Huang, H. T., Fiedler, H. E. and Wang, J. J., Limitation and Improvement of PIV, Part II: Particle Image Distortion, A Novel Technique, Exp. Fluids, 15 (1993), 263-273.

Lin, H. J. and Perlin, M., Improved methods for thin, surface boundary layer investigations, Exp. Fluids, 25 (1998), 431-444.

Mayer, S., A generalized processing technique in digital particle image velocimetry with direct estimation of velocity gradients, Exp. Fluids, 33 (2002) 443-457.

Md. Shafiquzzaman, Wells, J. C., Nanao, M., Kubo, M. and Nakajima, J., Attachment of Xanthomonas Maltophilus to Bioreactor Support Particles: Influence of Shear Stress and History Effects, Proceedings of the 38th Annual Convention of Japan Society on Water Environment (Hokkaido, Japan), (2004-3), 448.

Nguyen, C. V. and Wells, J. C., Investigation of near-wall coherent structures by stereo particle image velocimetry, Proceedings of FEDSM'03, 4th ASME-JSME Joint Fluids Engineering Conference (Hawaii, U.S.A.), (2003-7(a)).

Nguyen, C. V. and Wells, J. C., Measurement of wall velocity gradient in Stereo Particle Image Velocimetry, 54th Annual meeting of the A.P.S. Division of Fluid Dynamics (Rutherford, N.J., U.S.A.), (2003-11(b)).

Nguyen, C. V., Phan, N. M. T. and Wells, J. C., Deforming P.I.V. templates to measure interfacial velocity gradients, with extension to a stereo arrangement, Int. Conf. on Advanced Optical Diagnostics in Fluids, Solids and Combustion (Tokyo, Japan), (2004-12), V0045.

Okamoto, K., Nishio, S., Saga, T. and Kobayashi, T., Standard images for particle-image velocimetry, Meas. Sci. Technol., 11 (2000), 685-691.

Phan, N. M. T., Nguyen, C. V. and Wells, J. C., Direct Measurement of Surface-Normal Velocity Gradient at a Free Surface by Deforming PIV Templates, Proceedings, 6th World Conference on Experimental Heat Transfer, Fluid Mechanics, and Thermodynamics (Matsushima, Japan), (2005).

Ruan, X., Song, X. and Yamamoto, F., Direct measurement of vorticity field in digital particle images, Exp. Fluids, 30 (2001), 696-704.

Scarano, F., Iterative image deformation in PIV, Meas. Sci. and Technol., 13 (2002), R1-R19.

Tokumaru, P. T. and Dimotakis, P. E., Image correlation Velocimetry, Exp. Fluids 19, (1995), 1-15.

Wells, J. C, Sugimoto H, Nguyen, C. V. and Kishida, K., Camera calibration for stereo P.I.V. with a front-rear camera arrangement, application to open-channel flow, Annual Journal of Hydraulic Engineering, JSCE, 47 (2003).

Willert, C., Stereoscopic digital particle image velocimetry for application in wind tunnel flows, Meas. Sci. Technol., 8 (1997), 1465-1479.

Young, C. N., Johnson, D. A. and Weckman, E. J., A method to anchor displacement vectors to reduce uncertainty and improve particle image velocimetry results, Meas. Sci. Technol., 15 (2003), 9-20.

Author Profile

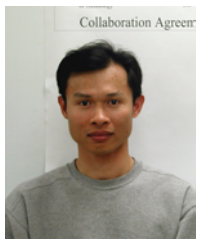

Chuong V. Nguyen: He received his B.Sc. in Aeronautical Engineering in 2001 from Ho Chi Minh City University of Technology, Vietnam. In 2003, he received his M.Sc. in Civil and Environmental Engineering from Ritsumeikan University, Japan. Currently he is a Ph.D candidate in the Department of Mechanical Engineering, Monash University, Australia. His research interests are PIV and Holographic PIV for wall-bounded flows.

John C. Wells: He obtained a Doctorate in Mechanics from the University of Grenoble I, France, and has worked at Ritsumeikan University as an Associate Professor in the Department of Civil and Environmental Engineering since 1999. His research interests are wall turbulence and sediment transport micromechanics.